Finite element models in the steel industry. Part I: simulation of flat product manufacturing processes

Eduardo N. Dvorkin, Miguel A. Cavaliere
and Marcela B. Goldschmit
Center for Industrial Research, FUDETEC
Av. Córdoba 320
1054, Buenos Aires, Argentina

Abstract

In this paper we discuss the finite element models that we developed for simulating several processes used for the production of flat steel products (plates and coils). In particular we discuss the modeling of steel continuous casting processes and of hot rolling processes.

1 Introduction

The first requirement for the development of a successful set-up and tight control of a production process is to have an in-depth knowledge of the process *technological windows*; that is to say, of the locus in the space of the process control variables, where the resulting products meet their specifications.

The task, that we face as engineers, is to *quantify* those technological windows. The possible ways for this quantification are:

- Industrial observations and measurements performed in situ, on the process that is being analyzed. This is a costly route because it involves using industrial installations as research labs. It is also very difficult in an industrial process to separate the effect of the different variables, because often it is not possible to make changes in one operational variable, keeping the rest of them constant.

- Lab scale models. It implies measuring on reduced scale models and afterwards translating the measurement results to the actual scale. This is also a costly and cumbersome route, since most of the physical phenomena to be quantified are nonlinear and it is not always possible to identify simple similarity relations.

- Computational models.

Computational models are nowadays a powerful and reliable tool for simulating different thermo-mechanical-metallurgical processes; hence, they are increasingly being used to investigate the technological windows of different processes in the steel industry, such as continuous casting, hot and cold rolling, heat treatments, etc. ([1] to [12]).

Since technological decisions, with high influence on the ecological impact of industrial facilities, on labor conditions and on revenues, are reached based on the results provided by numerical models, it is evident that these models have to be highly reliable. Therefore, it is of the highest importance that sound computational mechanics formulations are used [13], [14] and that the model results are subjected to experimental validation using either industrial or lab measurements.

In the development of computational models we have to recognize three different levels:

- The identification of the *physical problem* that is going to be analyzed and the isolation of its most relevant features. Here we have to make important decisions on which aspects of the process physics are relevant and, therefore, need to be considered in the model, and which aspects are not.

- The formulation of the *mathematical model*, usually in the form of a PDE system with its proper domain definition, boundary and initial conditions, etc. In this level we introduce hypotheses about the material response, about the friction description, etc. It is important that when an engineer analyzes the results provided by the mathematical model she/he checks the adequacy of those hypotheses.

- The formulation of a *numerical model*. In most cases the PDE system developed in the previous step cannot be solved in closed form; hence, it is necessary to get approximate solutions using a numerical method. In this paper we will focus on the finite element method.

A typical installation for manufacturing flat steel products (coils) is composed by a blast furnace (BF), a basic oxygen furnace (BOF), a continuous casting process and a hot rolling mill. Downstream the above facilities there is usually a cold rolling mill, annealing facilities, coating facilities, etc.[15]

The objective of this paper is to illustrate on actual industrial applications in which coil steel production processes are simulated using finite element models. For this purpose, in the second section we discuss the modeling of a continuous casting installation for steel slabs, in the third section we discuss the modeling of a hot rolling process and in the fourth section we discuss the constitutive relations that we use for simulating hot metal forming processes.

2 Modeling of the continuous casting process

Nowadays almost 90% of the world steel production is being produced in continuous casting installations [16], therefore this is a technology with a very high economical impact.

A schematic representation of a continuous casting installation for steel slabs is shown in Fig. 1, where we can identify the following sequence:

1. *The liquid steel is poured into a copper mold which is refrigerated with an external water jacket. The cooling of the steel and its solidification inside the mold progresses from the outside to the inside; therefore the external solidified steel shell increases its thickness as the steel strand transits the mold.*
   The physical process inside the mold is quite complex because the solidified steel shell and the mold are strained due to thermal and mechanical loads (ferrostatic pressure). While at the meniscus the steel is in contact with the mold internal surface, downstream a gap is opened between the strand and the mold and therefore there is more resistance to the heat exchange. However, in some cases, the mold is shaped so as to regain its contact with the strand at its lower sections.
   Usually the slab molds are equipped with thermocouples located through the thickness of its copper plates, the indications of these thermocouples are the input to a heuristic algorithm that provides break-out alarms.
   The mathematical description of the heat transfer between the strand and the mold requires a model that couples the heat transfer equations with the description of the mold thermo-mechanical deformations.
   An alternative procedure is to use an empirical law that describes the heat flow between the steel strand and the mold, e.g. the Savage-Pritchard [17] equation and its modifications proposed by Brimacombe and coworkers [18]. It has been shown that this empirical approach may introduce important deviations between the model predictions and the actual temperatures distribution (see section 2.1.2).
   Another alternative, that we develop in the present paper, is to use the indications of the mold thermocouples to evaluate, via an inverse analysis procedure, the heat transfer coefficients that govern the thermal process in the mold; in this way an uncoupled heat transfer analysis can be performed.

2. *The steel strand exits the mold and continues its solidification. The distance, measured along the slab centerline, between the meniscus and the section at which the strand solidification is completed is called the "metallurgical length".*
   After exiting the mold the steel strand is cooled with water jets and also by interchanging heat with refrigerated guide rolls.

In our Ref.[19] we developed the computer system CCAST composed by two modules:

- The module CCAST-D, which is a finite element code that, with the information of the heat fluxes between the strand and the mold, solves the thermal problem in the strand.

- The module CCAST-I which evaluates the heat exchange between the strand and the mold.

The heat exchange strand / mold is modelled as,

$$q_{steel/mold} = h_{steel/mold}\,(T_{mold} - T_{steel}) \tag{1}$$

where at a given point $q_{steel/mold}$ is the heat flux, $h_{steel/mold}$ is the corresponding heat transfer coefficient, T_{steel} is the strand surface temperature and T_{mold} is the corresponding mold inner surface temperature.

The values of $h_{steel/mold}$ are interpolated from a finite number of values $h_{steel/mold}\big|_k$ with $k = 1, ..., NCOEF$. These $NCOEF$ values are the unknown in our inverse analysis procedure (CCAST-I).

The objective is to produce a set of values, $\left[h_{steel/mold}\right]$ that when introduced in between the finite element models of the steel strand and the copper mold predict:

- At the NTH thermocouple locations the same temperatures that the ones registered during the actual continuous casting process.

- The same temperature increase in the mold cooling water that the one registered during the actual continuous casting process.

The above described conditions lead to a system of $(NTH + 1)$ linear equations with $NCOEF$ unknowns, being $NCOEF > (NTH + 1)$ the system has multiple solutions. We can write the resulting system as,

$$[A]\left[h_{steel/mold}\right] = [b] \tag{2}$$

In order to select, among the multiple solutions, the solution that better fulfils the physics of our problem in Ref. [19] we established the following minimization problem to be solved under the constraints imposed by Eqns. (2),

$$minimize \quad \left[\begin{array}{c} \frac{1}{2}(\left\| \left[h_{steel/mold}\right] \right\|^2 + \left\| \underline{\underline{L}}^{MAX}(\left[h_{steel/mold}\right]) \right\|^2 + \\ \alpha^2 \sum_i \langle g_i \rangle + \left\| \underline{\underline{L}}^{SMT}(\left[h_{steel/mold}\right]) \right\|^2) \end{array} \right] \tag{3}$$

In the above,

- The first term inside the parentheses on the r.h.s. imposes the condition that from all possible solutions we choose the solution with the minimum norm.

- The second and third terms inside the parentheses on the r.h.s. imposes an *a priori information*: at the meniscus level the heat flux presents a maximum. The second term imposes the necessary condition for an extreme.

- The interpolation functions adopted for the heat transfer coefficient are piece-wise constant, therefore to calculate the derivatives in the above equation we use a finite difference operator: the matrix $\underline{\underline{L}}^{MAX}$.

- However, we also have to impose the sufficient condition for a maximum. This condition can be written for every element containing the meniscus level as,

$$g_i = (h_{steel/mold,j} - h_{steel/mold,i}) \leq 0 \, . \tag{4}$$

  In the above equation the $i-$level is on the meniscus and the $j-$level is immediately below.
  Also α^2 is a penalty factor to be determined by numerical experimentation and $\langle \cdot \rangle$ are the Macauley brackets.

- The fourth term inside the parentheses on the r.h.s. imposes another a priori information: the heat transfer coefficient has to be a smooth function. Hence, we impose,

$$minimize \quad \left\| \nabla^2 \underline{h}_{steel/mold} \right\|^2 \, . \tag{5}$$

  In order to calculate the Laplacian in Eqn.(5) we use a finite difference operator: the matrix $\underline{\underline{L}}^{SMT}$.

In Ref. [19] we developed a numerical methodology for the iterative solution of the constrained minimization problem described by Eqns. (3) and (2).

2.1 Numerical simulations using CCAST

2.1.1 Stability test

We need to test the stability of the solutions provided by the CCAST system; for this purpose we consider a set of thermocouple indications obtained during a period of time in which the set up of the operational variables was stationary. For each thermocouple we consider its average indication and its standard deviation and then we run two analyses:

1. Using the average indication for each thermocouple.

2. Using a modified set of values, each thermocouple indication was modified using a random error proportional to its standard deviation:

$$\begin{aligned} T_i^{\varepsilon} &= T_i^{average} + 3\,\varepsilon\, s_i \\ -1 &\leq \varepsilon \leq 1 \ \textit{random variable} \\ s_i &: \textit{standard deviation of the set of thermocouple indications for } T_i \, . \end{aligned}$$

Also,

$$\begin{aligned} G^{\varepsilon}_{water} &= G^{average}_{water} + 3\,\varepsilon\; s_{GW} \\ \Delta T^{\varepsilon}_{water} &= \Delta T^{average}_{water} + 3\,\varepsilon\; s_{TW}. \end{aligned}$$

In Fig. 2 we compare the results of both analyses for one thermocouple line (TC4). It can be observed that the results corresponding to the average and perturbed set of values are almost coincident; therefore, we can assess that the developed algorithm (CCAST-D + CCAST-I) provides very stable results.

2.1.2 Analysis of an industrial case

We use the CCAST system with the information provided by the thermocouples installed in a mold of SIDERAR continuous casting facility (San Nicolás, Argentina).

The thermocouples data correspond to the average of the data acquired during a period of 28 min.

The casted steel chemical composition is indicated in Table I.

%**C**	%**Mn**	%**Si**	%**P**	%**S**	%**Al**
0.07	0.25	0.03	0.02	0.015	0.035

Table I

In Fig. 3 we show the temperature map predicted by the system for the hot face of the mold movable plate. This map does not show a uniform temperature distribution due to the geometries of the water cooling channels and of the mold structure. Notice that the temperatures increase near the mold exit due to the lack of cooling water in this area of the analyzed mold [20]. In Fig. 4 we represent the steel / mold heat fluxes predicted by our model.

In Fig. 5 we compare the phase distribution results that were obtained, in a section located 800 mm downstream the meniscus, using:

- The complete CCAST system including the inverse analysis module.
- CCAST-D with the steel / mold heat fluxes provided by the Savage-Pritchard equation adjusted to match the total heat extraction measured in the actual mold.

In Fig. 6 we present a detailed comparison of the corner areas. The difference in these areas, at the mold exit, is as large as $300^{\circ}C$; this result indicates that the Savage-Pritchard equation does not provide a good approximation in those areas where the gap is larger. Similar results have been reported in Ref.[21].

3 Modeling of the hot rolling process

In previous references we developed a formulation for modeling bulk metal forming processes based on the flow formulation [22](rigid - viscoplastic material models) and the pseudo-concentrations technique [23], [24]. The resulting formulation uses an Eulerian description of motion inside a fixed mesh avoiding, therefore, the numerical problems associated with the re-meshing procedures that are required when a Lagrangian description of motion is used.

We implemented the above mentioned finite element formulation in our code METFOR. When specialized for the analysis of hot rolling processes our formulation couples the rigid-viscoplastic deformation of the workpiece to the elastic deformation of the rolls. The heating and thermal expansion of the rolls are also incorporated into the formulation.

A description of the application of our finite element formulation to the analysis of hot rolling processes, together with experimental validation of the numerical results and a discussion of technological applications can be found in our Refs. [2], [5], [8] and [11].

3.1 Numerical simulation of an industrial case

In Fig. 7 we present a schematic representation of the hot rolling mill at Sidor (Puerto Ordaz, Venezuela) and in what follows we show the results of a parametric study that we carried out for the finishing stand F1.

The temperature map of the working rolls changes during the rolling process, each coil is processed with a different working rolls temperature map; even more, the rolls temperature map changes from the beginning to the end of a coil process. Hence, we focus our study on the rolling conditions of a selected coil.

In Fig. 8.a we present two temperature maps of the F1 working rolls, one corresponding to the beginning of the selected coil process and the second one corresponding to the finish of the selected coil process; it is clearly shown the evolution of the temperature map during the process of a single coil. In Fig. 8.b we present the rolls profile[1] at the same instants.

In Fig. 9 we present the fixed mesh that we used for modeling the F1 stand and the pseudo-concentrations distribution (the actual material corresponds to the shaded space).

Finally in Fig. 10 we present the results of our parametric study, showing the profile of the plate[2] that exits the stand F1 under three conditions:

- Working rolls with their mechanical and thermal crown considered [3].
- Working rolls with only the mechanical crown (beginning of the rolling process with cold rolls)

[1] See Appendix
[2] See Appendix
[3] See Appendix

- Working rolls without mechanical crown and with the corresponding thermal crown.

4 Material constitutive relations for modeling hot steel forming processes

When modeling hot metal forming processes using rigid-viscoplastic material models we use an associate viscoplastic flow rule with von Mises yield function [25]. Also an isotropic hardening law is normally used to relate the instantaneous yield stress (σ_y) with the equivalent viscoplastic strain ($\overline{\varepsilon}$), the equivalent viscoplastic strain rate ($\dot{\overline{\varepsilon}}$) and the temperature ($T$),

$$\sigma_y = \sigma_y(\overline{\varepsilon}, \dot{\overline{\varepsilon}}, T) \tag{6a}$$

$$\dot{\overline{\varepsilon}} = \frac{D\,\overline{\varepsilon}}{D\,t} = \sqrt{\frac{2}{3}\,\dot{\varepsilon}_{ij}\,\dot{\varepsilon}_{ij}} \tag{6b}$$

where, $\dot{\varepsilon}_{ij}$ are the components of the strain rate tensor and $\frac{D(.)}{Dt}$ is a material derivative [26].

In the present section we are going to assume *instantaneous plasticity*; hence, we can write for the equivalent von Mises stress ($\overline{\sigma}$) [25],

$$\overline{\sigma} = \sigma_y = \sigma_y(\overline{\varepsilon}, \dot{\overline{\varepsilon}}, T)\ . \tag{7}$$

For defining the above relation we can follow two main approaches:

- *Phenomenological constitutive relations.* Curve fitting of simple mechanical tests are used to determine the material parameters involved in these constitutive relations (e.g. torsion, tension or compression tests).
- *Constitutive relations based on the modeling of the microstructural evolution.* These constitutive relations are based on more fundamental physical bases and the material parameters to be adjusted are determined via microstructural observations in programmed temperature - deformation excursions.

In the present section we will discuss three different phenomenological hardening laws and we will comment on its limitations to accurately represent the behavior of a steel being deformed at high temperature. We will also discuss an algorithm for identifying the parameters used in the phenomenological constitutive equations from the results of the torsion test.

4.1 Phenomenological constitutive relations

In Ref. [27] the Author reviews different phenomenological models, used when modeling hot metal forming processes, for computing the instantaneous yield stress as a function of the deformation parameters and the temperature (6a).

In this section we will concentrate our discussion on three strain hardening models: The Fields - Backofen model and two exponential-power models.

- *The Fields - Backofen model*

$$\sigma_y = A(T)\ \overline{\varepsilon}^{n(T)}\ \dot{\overline{\varepsilon}}^{m(T)} \quad . \tag{8}$$

This model provides, for a fixed temperature and a fixed viscoplastic strain rate, an yield stress that monotonically grows with the equivalent viscoplastic strain; hence, it cannot represent recrystallization phenomena ([28], [29]) such as the one illustrated in Fig. 11 for a set of compression tests performed on steel samples at our metallurgical lab and post-processed to obtain the *true stress - true strain* curves as indicated in Ref. [30].

For any material to be considered, and for each temperature level to be considered we have to determine the following material constants: $A(T), n(T),\ m(T)$.

- *Exponential-power law 1*

$$\sigma_y = [A(T)\ e^{-B(T)\overline{\varepsilon}}\ (\overline{\varepsilon} + \overline{\varepsilon}_o)^{n(T)} + C(T)\ (1 - e^{-B(T)\overline{\varepsilon}})]\ \dot{\overline{\varepsilon}}^{m(T)} \quad . \tag{9}$$

This law takes the functional form,

$$\sigma_y = f\ (\overline{\varepsilon}, T)\ g(\dot{\overline{\varepsilon}}) \ . \tag{10}$$

For a test at constant temperature and constant strain rate, since $g(\dot{\overline{\varepsilon}}) \neq 0$, the maximum stress (see Fig. 11) will be located at a strain value $\overline{\varepsilon}^*$given by the following equation,

$$\frac{\partial f}{\partial \overline{\varepsilon}} = 0 \tag{11}$$

therefore, $\overline{\varepsilon}^*$ will not be a function of $\dot{\overline{\varepsilon}}$. This behavior does not match the experimental evidence shown in Fig. 11, from which it is clear that the strain value that defines the stress peak ($\overline{\varepsilon}^*$) grows with the strain rate. Even tough a definition of a constitutive relation that can accommodate the relation $\overline{\varepsilon}^* = \overline{\varepsilon}^*(\dot{\overline{\varepsilon}})$ is most desirable, the above defined exponential-power law has proved to provide very good results in the modeling of hot rolling processes.

For any material to be considered, and for each temperature level to be considered we have to determine the following material constants: $A(T)$, $B(T)$, $C(T)$, ε_o, $n(T)$, $m(T)$.

We also define the following temperature dependence:

$$\begin{aligned} A(T) &= K_o\, e^{\frac{\beta}{T}} \\ B(T) &= (r_o + r_1 T) \\ C(T) &= K_{st}\, e^{\frac{\beta_{st}}{T}} \\ n(T) &= n_o \\ m(T) &= m_o + m_1 T \end{aligned} \tag{12}$$

- *Exponential-power law 2*

$$\sigma_y = [A(T)\, e^{-B(T)\overline{\varepsilon}}\, \sqrt{(1 - e^{-n(T)(\overline{\varepsilon}+\overline{\varepsilon}_o)})} + C(T)\, (1 - e^{-B(T)\overline{\varepsilon}})]\dot{\overline{\varepsilon}}^{\,m(T)} \quad . \tag{13}$$

For this case we have the same comments as for the previous one.

For any material to be considered, and for each temperature level to be considered we have to determine the following material constants: $A(T)$, $B(T)$, $C(T)$, ε_o, $n(T)$, $m(T)$.

We define the same temperature dependence as for the *exponential-power law 1.*

4.2 Mechanical tests used for material parameters identification

There are basically three simple mechanical tests that can be independently used to determine the material parameters defined above when describing the phenomenological hardening models: the tension test, the compression test and the torsion test.

The tension test presents the problem of the varying geometry of the sample during necking; hence, it is normally used in the range of small strains, a range that is not useful for the modeling of hot metal forming processes.

For the compression test with logarithmic strains smaller than (-0.8) the bulging of the sample, induced by the friction between the sample and the compression dies, affects the results; since the friction coefficient between the sample and the compression dies is normally not known, this test is also used in the range of relatively small strains, a range that is not useful for the modeling of hot metal forming processes [30].

The torsion test provides data for the complete strain range that is of interest when modeling hot metal forming processes, therefore we will concentrate on this test [31].

4.3 Post-processing the torsion test for material parameters identification

In what follows we present an algorithm for identifying the material parameters, for any of the three strain hardening laws described in the previous subsection, using the torque - turn curves produced with a set of torsion tests.

In Fig. 12 we show the experimental torque-turn curves obtained at a fixed temperature and using different angular velocities.

By performing the inverse analysis that we will describe in what follows we can identify for each material model the corresponding parameters. Using the calculated parameters we can calculate the resulting values of Γ_{ANA}, which we plot in the same figure.

In what follows we call,

Γ : torque

N : turns

$\dot{N}$: turns per unit time ($\frac{dN}{dt}$).

Each curve $\Gamma = \Gamma(N)$ corresponds to a fix set $(\dot{N}, T)$.

We start our identification algorithm defining the torque, in a round solid specimen with radius (R) and length (L), as a function of the equivalent stress,

$$\Gamma(N, \dot{N}) = \frac{2\pi}{\sqrt{3}} \int_0^R \overline{\sigma}(\overline{\varepsilon}, \dot{\overline{\varepsilon}})\, r^2\, dr \tag{14a}$$

$$\overline{\varepsilon} = \frac{2\pi r}{\sqrt{3}L} N \tag{14b}$$

$$\dot{\overline{\varepsilon}} = \frac{2\pi r}{\sqrt{3}L} \dot{N}\ . \tag{14c}$$

Using one of the phenomenological constitutive equations defined in the previous section, we can calculate for any set of values $(N, \dot{N}, T)$, using Eqns. (14a to 14c), an analytical value for the torque (Γ_{ANA}). Being $[X_i]$ the vector of material constants corresponding to a given phenomenological constitutive equation and to a temperature (T), we can write,

$$\Gamma_{ANA} = \Gamma_{ANA}(N, \dot{N}, X_i)\ . \tag{15}$$

- *For the Fields - Backofen model,*

$$\Gamma_{ANA} = \frac{2\pi}{\sqrt{3}} \int_0^R A \left(\frac{2\pi}{\sqrt{3}L} Nr\right)^n \left(\frac{2\pi}{\sqrt{3}L} \dot{N} r\right)^m r^2\, dr \tag{16}$$

$$= \frac{2\pi}{\sqrt{3}} \frac{A \left(\frac{2\pi}{\sqrt{3}L} NR\right)^n \left(\frac{2\pi}{\sqrt{3}L} \dot{N} R\right)^m R^3}{n+m+3}\ .$$

- *For the exponential-power law 1 model,*

$$\Gamma_{ANA} = \frac{2\pi}{\sqrt{3}} \int_0^R \left[A \left(\frac{2\pi}{\sqrt{3}L} Nr \right)^n e^{-B\frac{2\pi}{\sqrt{3}L}Nr} + C(1 - e^{-B\frac{2\pi}{\sqrt{3}L}Nr}) \right] \left(\frac{2\pi}{\sqrt{3}L} \dot{N}r \right)^m r^2 \, dr \, . \quad (17)$$

Notes:

1. From direct inspection of the experimental curves we set $\varepsilon_o = 0$.
2. We do not get a closed form solution of the integral in the above equation; therefore, we work with numerical integrals.

- *For the exponential-power law 2 model,*

$$\Gamma_{ANA} = \frac{2\pi}{\sqrt{3}} \int_0^R \left[A \sqrt{1 - e^{-n\frac{2\pi}{\sqrt{3}L}Nr}} \, e^{-B\frac{2\pi}{\sqrt{3}L}Nr} + C(1 - e^{-B\frac{2\pi}{\sqrt{3}L}Nr}) \right] \left(\frac{2\pi}{\sqrt{3}L} \dot{N}r \right)^m r^2 \, dr \, . \quad (18)$$

Same notes as for the previous case.
We now define for the considered temperature an error function,

$$E(X_i) = \sum_N \sum_{\dot{N}} [\Gamma_{ANA}(N, \dot{N}, X_i) - \Gamma_{EXP}(N, \dot{N}, T)]^2 \, . \quad (19)$$

As a first step we minimize the above defined error function, obtaining the material parameters $[X_i]$ corresponding to each tested temperature; afterwards we use Eqns. (12) or similar ones to establish the temperature dependence of the material parameters.

It is important to remark that in the case of the exponential-power laws we could have used Eqns. (12) in Eqns. (17) and (18) obtaining; therefore, a system wit 10 equations. We chose to solve several systems of 5 equations (one for each tested temperature) rather than one system of 10 equations due to the bad conditioning of the system, typical of inverse problems.

4.3.1 The Fields-Backofen model

In this case we can simplify the error minimization by redefining the error function as,

$$E(X_i) = \sum_N \sum_{\dot{N}} [\ln \Gamma_{ANA}(N, \dot{N}, X_i) - \ln \Gamma_{EXP}(N, \dot{N}, T)]^2 \, . \quad (20)$$

The minimization of the above error function leads to a nonlinear system of equations.

4.3.2 The exponential-power law models

In these cases the integrals involved in the definition of Γ_{ANA} are calculated using the Gauss numerical integration method, therefore we make the following variable transformation,

$$r \,\epsilon\, [0, R] \rightarrow \xi \,\epsilon\, [-1, 1] \tag{21}$$

where the coordinate value "ξ" is called *natural coordinate*.

Hence, for Eqn. (17) we get,

$$\Gamma_{ANA} = \frac{2\pi}{\sqrt{3}} \sum_{i=1}^{NGAUS} w_i \left[A\, \varepsilon_i^n\, e^{-B\varepsilon_i} + C(1 - e^{-B\varepsilon_i})\right] \dot{\varepsilon}_i^m \left[\frac{R}{2}(1 + \xi_i)\right]^2 \frac{R}{2} \tag{22}$$

and for Eqn. (18) we get,

$$\Gamma_{ANA} = \frac{2\pi}{\sqrt{3}} \sum_{i=1}^{NGAUS} w_i \left[A \sqrt{1 - e^{-n\varepsilon_i}}\, e^{-B\varepsilon_i} + C(1 - e^{-B\varepsilon_i})\right] \dot{\varepsilon}_i^m \left[\frac{R}{2}(1 + \xi_i)\right]^2 \frac{R}{2}\,. \tag{23}$$

In the above equations,

$NGAUS$: number of Gauss points used for the numerical integration.

$\varepsilon_i = \frac{\pi R}{\sqrt{3}L} N\ (1 + \xi_i)$

$\dot{\varepsilon}_i = \frac{\pi R}{\sqrt{3}L} \dot{N}\ (1 + \xi_i)$

w_i is the weight associated to the *i-th* integration point and ξ_i is its natural coordinate.

4.3.3 Inverse analysis

For any of the three constitutive laws and for a fixed temperature T the set of material parameters that *best approximates* the experimental curves is $\left[\widehat{X}_i\right]$ for $i = 1, ..., NPAR$ ($NPAR = 3$, for the Fields - Backofen model and $NPAR = 5$ for the exponential - power models); hence, the error is minimum (not necessarily zero) for this set of parameters:

$$\left[\frac{\partial E}{\partial X_i}\right]_{\widehat{X}} = 0 \quad i = 1, ..., NPAR \tag{24}$$

Using as a starting set $[X]^{(0)}$, we solve the nonlinear equations system (24) with an iterative procedure that for the *k-th* iteration can be written as,

$$\left[\frac{\partial E}{\partial X_i}\right]^{(k-1)} + \left[\frac{\partial^2 E}{\partial X_i\, \partial X_j}\right]^{(k-1)} [\Delta X_j]^{(k)} = 0 \;\; i = 1, ..., NPAR \tag{25a}$$

$$[X_i]^{(k)} = [X_i]^{(k-1)} + \beta \;\; [\Delta X_j]^{(k)} \quad i = 1, ..., NPAR \; . \tag{25b}$$

In Eqn. (25a) the repeated subindex "j" indicates a sum from one to $NPAR$; the value β is obtained using a standard *line search* algorithm [32].

The iterative process is continued until,

$$\left\| \left[\frac{\partial E}{\partial X_i}\right]^{(k)} \right\| \leq ETOL \; . \tag{26}$$

Notice that for the Fields - Backofen model the first and second derivatives in Eqn.(25a) can be calculated using a closed form expression while for the exponential - power models these first and second derivatives are calculated deriving Eqns.(22) or (23).

Our numerical experimentation shows that for the case of the exponential - power material models the Newton iterative procedure in Eqns. (25a,25b) is not *globally convergent* [32], that is to say not every starting set $[X]^{(0)}$ will provide a converged solution. Also, due to the bad conditioning of the system, starting from different points we may get different solutions satisfying the inequality in (26). Hence, for the case of the exponential - power models, we developed a separate algorithm for producing a convenient estimation of the starting set.

4.3.4 Inverse analysis: Definition of a starting set for the exponential - power material models

In this algorithm we take into account:

1. The experimentally determined value of $\Gamma_\infty = \lim_{N \to \infty} \Gamma(N)$ (see Fig. 12) that will be used to determine the constants C and m. For both exponential - power models,

$$\lim_{N \to \infty} \Gamma_{ANA} = \frac{2\pi}{\sqrt{3}} \; C \; \left(\frac{2\pi}{\sqrt{3}} \dot{N} \; \frac{R}{L}\right)^m \frac{R^3}{m+3} \tag{27}$$

the initial values of (C, m) will minimize the function

$$\begin{aligned} E\Gamma(C,m) &= \sum_{\dot{N}} (\ln \Gamma_\infty^{ANA} - \ln \Gamma_\infty^{EXP})^2 \qquad (28) \\ &= \sum_{\dot{N}} \left[(\ln(\frac{2\pi}{\sqrt{3}} \; C \; R^3) + m \; \ln(\frac{2\pi}{\sqrt{3}} \dot{N} \; \frac{R}{L}) - \ln(m+3) - \ln \Gamma_\infty^{EXP} \right]^2 \end{aligned}$$

2. The value $\widehat{N}$ that corresponds to the peak torque satisfies the equation $\left[\frac{\partial \Gamma}{\partial N}\right]_{\widehat{N}} = 0$. In the torque analytical expression the value $\Lambda_{ANA} = \Gamma_{ANA}/\dot{N}^{m}$ is independent of $\dot{N}$ (see Eqns. (22) and (23)); however in the experimental curves this is not necessarily the case. Hence, we take as $\left(\widehat{\Lambda}_{EXP}, \widehat{N}_{EXP}\right)$ the average of the corresponding magnitudes on the curves obtained at constant rotation speed.

$$\widehat{\Lambda}_{EXP} = \frac{1}{NTOT} \sum_{i=1}^{NTOT} \left[\frac{\widehat{\Gamma}_{EXP}}{\dot{N}^{m}}\right]_i \tag{29a}$$

$$\widehat{N}_{EXP} = \frac{1}{NTOT} \sum_{i=1}^{NTOT} \left[\widehat{N}_{EXP}\right]_i \tag{29b}$$

The two equations that we use to determine admissible set of starting values (A, B, n) are,

$$\widehat{\Lambda}_{ANA} = \widehat{\Lambda}_{EXP} \tag{30a}$$

$$\left[\frac{\partial \widehat{\Lambda}_{ANA}}{\partial N}\right]_{\widehat{N}_{EXP}} = 0 \tag{30b}$$

To define the starting set of parameters:

- We use the values of (C, m) obtained from the minimization of the function defined by Eqn. (28).
- We define with Eqns. (30a,30b) the relations $A = A(n)$ and $B = B(n)$ and afterwards we search the value of $n \in [0, n_{MAX}]$ that produces the smaller error E (Eqn.(19)) within the discrete set of values $\left[0, \frac{n_{MAX}}{NS}, 2\frac{n_{MAX}}{NS}, ..., n_{MAX}\right]$. From practical considerations we use $n_{MAX} = 1$ for the first exponential - power model and $n_{MAX} = 10$ for the second one and $NS = 10$.

4.3.5 Inverse analysis results

The experimental tests shown in Fig. 12 were also performed at different temperatures. In Figs. 13-15 we represent the $\overline{\sigma} - \overline{\varepsilon}$ curves that we obtained post-processing the torsion tests with each of the considered phenomenological material models.

Please notice that,

- As commented above the Fields - Backofen law fails to represent the recrystallization phenomenon observed in the experimental curves.
- The Exponential Power Laws 1 and 2 while representing the recrystallization phenomenon are not able to represent the strain-rate induced shifting of the peak stress location.

- Since the problem of determining the material constants by fitting the torque - turn experimental curves is ill conditioned, the solution is not unique; hence, we may get different sets of parameters providing approximately the same torque-turn analytical curves and the same stress - strain curves.

5 Conclusions

In the present paper we discussed the application of the finite element method to the modeling of the manufacturing processes for flat steel products (plates and coils).

Since numerical model results are nowadays used in industry as the basis for fundamental technological decisions, it is very important that the numerical models are as accurate as possible; therefore, the analysts should select finite element formulations that guarantee convergence when the mesh is refined and stability when boundary conditions or material properties are changed (see [14] and [13]).

Another fundamental issue is the use of accurate values for the physical properties. Related to this are the inverse analysis procedures used for parameters identification. Considering that these procedures are normally ill-conditioned, it is very important to introduce in them as much physical knowledge as possible, in order to "guide" the solution.

Acknowledgment. *We gratefully acknowledge the support of the Techint Steel Sector for this research.*

References

[1] E.N.Dvorkin, "Computational modelling for the steel industry at CINI", *IACM-Expressions*, N°10, 2001.

[2] M.A.Cavaliere, M.B.Goldschmit and E.N.Dvorkin, "Finite element simulation of the steel plates hot rolling process", *Int. J. Numerical Methods in Engng.*, **52**, pp.1411-1430, 2001.

[3] M.B. Goldschmit and A.H. Coppola Owen, "Numerical modeling of gas stirred ladles", *Ironmaking & Steelmaking*, **28**, 337-341, 2001.

[4] M.B. Goldschmit, S.P. Ferro, G.F. Walter, V.G. Aranda and J.A. Tena Morelos, "Numerical model for the minization of intermixed round bars in a four line continuous caster", *Met. And Mat. Transactions B*, **32B**, pp.537-546, 2001.

[5] M.A.Cavaliere, M.B.Goldschmit and E.N.Dvorkin, "Finite element analysis of steel rolling processes", *Computers & Structures*, **79**, pp.2075-2089, 2001.

[6] M. Maldovan, J. Príncipe, G. Sánchez, A. Pignotti y M. Goldschmit, "Numerical modeling of continuous casting of rounds with electromagnetic stirring", *Proceedings European Congress on Computational Methods in Applied Sciences and Engineering - ECCOMAS 2000*, Barcelona, España, 2000.

[7] M.B. Goldschmit, R. J. Príncipe and M. Koslowski, "Applications of a (k-ε) model for the analysis of continuous casting processes", *International Journal for Numerical Methods in Engineering*, **46**,1505-1519, 1999.

[8] E.N.Dvorkin, M.A.Cavaliere, M.B.Goldschmit and P.M.Amenta, "On the modeling of steel product rolling processes", *Int.J.Forming Processes (ESAFORM)*, **1**, pp.211-242, 1998.

[9] M.B. Goldschmit, R.J. Príncipe and M. Koslowski, "Numerical modeling of submerged entry nozzle", *Proceedings 3rd. European Conference on Continuous Casting*, Madrid, October 1998.

[10] M.B. Goldschmit, "Computational fluid mechanics applications in continuous casting", *Proceedings 80th Steelmaking Conference*, Chicago, EEUU, 1997.

[11] E.N.Dvorkin, M.B.Goldschmit, M.A.Cavaliere, P.M.Amenta, O.Marini and W.Stroppiana, "2D finite element parametric studies of the flat rolling process", *J. of Materials Processing Technology*, **68**, pp.99-107, 1997.

[12] M.B. Goldschmit, J.C. González and E.N. Dvorkin, "On a finite element model for analyzing the liquid slag development during continuous casting of round bars", *Ironmaking & Steelmaking*, **20**, N° 5, 379-385, 1993.

[13] K.J.Bathe, *Finite Element Procedures*, Prentice Hall, Upper Saddle River N.J., 1996.

[14] E.N.Dvorkin, "On the convergence of incompressible finite element formulations: the Patch Test and the Inf-Sup condition", *Engng. Computations*, **18**, pp.539-556, 2001.

[15] *The Making, Shaping and Treating of Steel* (W.T.lankford, N.L.Samways, R.F.Craven and H.E.McGannon Eds.), U.S.Steel,10th. Edition, 1985.

[16] M.M.Wolf, "Historical aspects and key technologies", *The Making, Shaping and Treating of Steel*, (Ironmaking Volume, 11th. Edition), AISE Steel Foundation, (in press).

[17] J.Savage and W.H.Pritchard, The problem of rupture of the billet in the continuous casting of steel, *J. Iron and Steel Inst.*, pp.269-277, November 1954.

[18] J.E.Lait, J.K.Brimacombe and F.Weinberg, Mathematical modelling of heat flow in the continuous casting of steel, *Ironmaking and Steelmaking (Quarterly),* **2**, pp.90-97, 1974.

[19] M.Gonzalez, M.B.Goldschmit, A.P.Assanelli, Elena Fernández Berdaguer and E.N.Dvorkin, "Modeling of the solidification process in a continuous casting installation for steel slabs", (submitted)

[20] I.V.Samarasekera and J.K.Brimacombe,"Investigation of mold related quality problems in continuous billet casting using mathematical models", *Proceedings Third PTD Conference on Application of Mathematical and Physical Models in the Iron and Steelmaking Industry*, IIS, Pittsburgh, pp.283-295, 1982.

[21] B.G.Thomas, G.Li, A.Moita and D.Habing, "Analysis of the thermal and mechanical behavior of the copper molds during continuous casting of steel slabs", *ISS Transactions,* pp. 125-143, 1998.

[22] O.C.Zienkiewicz, P.C.Jain and E.Oñate, "Flow of solids during forming and extrusion: some aspects of numerical solutions", *Int.J.Solid Struct.*, **14**, pp.15-28, 1977.

[23] E.N.Dvorkin and E.G.Petöcz, "An effective technique for modelling 2D metal forming processes using an Eulerian formulation", *Engng. Computations*, **10**, pp.323-336, 1993.

[24] E.N.Dvorkin, M.A.Cavaliere and M.B.Goldschmit, "A three field element via augmented lagrangian for modelling bulk metal forming processes", *Computational Mechanics*, **17**, pp.2-9, 1995.

[25] P.Perzyna, "Fundamental problems in viscoplasticity", *Advances in Applied Mechanics*, **9**, Academic Press, 1966.

[26] L.E.Malvern, *Introduction to the Mechanics of a Continuous Medium*, Prentice-Hall, Englewood Cliffs, NJ, 1969.

[27] Z.Gronostajski, "The constitutive equations for FEM analysis", *J. of Materials Processing Technology,* **106**, pp.40-44, 2000.

[28] W.A.Backofen, *Deformation Processing*, Addison-Wesley, Reading MA, 1972.

[29] G.E.Dieter, *Mechanical Metallurgy,* McGraw Hill, 1986.

[30] M.A.Cavaliere, G.Gómez, J.I.Gazzarri, T.E.Pérez and E.N.Dvorkin, "Experimental procedure for determining true stress - true strain curves for steels in the high temperature range and under controled deformation rate", *Proceedings ECCOMAS 2000 (European Congress on Computational Methods in Applied Sciences and Engineering) - COMPLAS VI (Sixth Int. Conf. on Computational Plasticity)*, Barcelona, CIMNE, 2000.

[31] D.S.Fields and W.A.Backofen, "Determination of strain hardening characteristics by torsion testing", *Proc. ASTM,* **57**, pp.1259-1271, 1957.

[32] Luenberger D.G., *Linear and Nonlinear Programming*, Addison-Weley, Reading MA, 1984.

A Rolling terminology

In this appendix we are going to briefly comment some concepts pertaining to rolling technology, that have been used in the main body of this paper.

A.1 Plate profile and plate crown

The transversal section of a rolled steel plate is usually not a rectangle but it has a shape similar to the one schematized in Fig. 16, this shape is referred to as the *plate profile*. In order to have a quantitative measure of the difference between the plate thickness at the center of its transversal section and near its edges the *plate crown* is defined; in the same figure we indicate this definition.

A.2 Plate flatness

Since the transversal section of a plate is of variable thickness, it is apparent that during rolling different fibers located at different locations across the plate will undergo different elongations; hence, due to the plate continuity, some fibers will be in a tensile state and others in a compressive state. It is well known that the compressed parts may buckle and therefore the plate may loose its *flatness*.

A.3 Rolls profile and crown

The work rolls and sometimes also the back-up rolls are not straight cylinders, usually the cylinder generatrices have a shape similar to the ones indicated in Fig. 17 (*roll profiles*), to compensate the bending of the rolls and therefore produce a plate with a smaller crown. The number used to define a roll profile is the *roll crown* whose definition is also indicated in the same figure.

As it was discussed in the fourth section the thermal evolution of the work rolls during rolling imposes an evolution of their shape, hence the original or *mechanical crown* of the rolls is modified by a *thermal crown*; therefore,

$$\textit{total crown} = \textit{mechanical crown} + \textit{thermal crown}$$

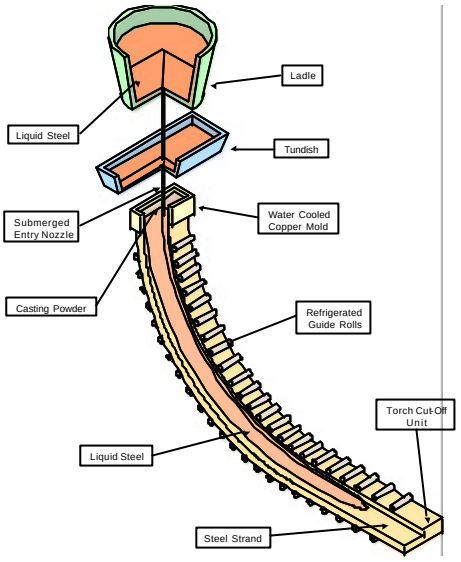

Figure 1: Scheme of a continuous casting installation for steel slabs

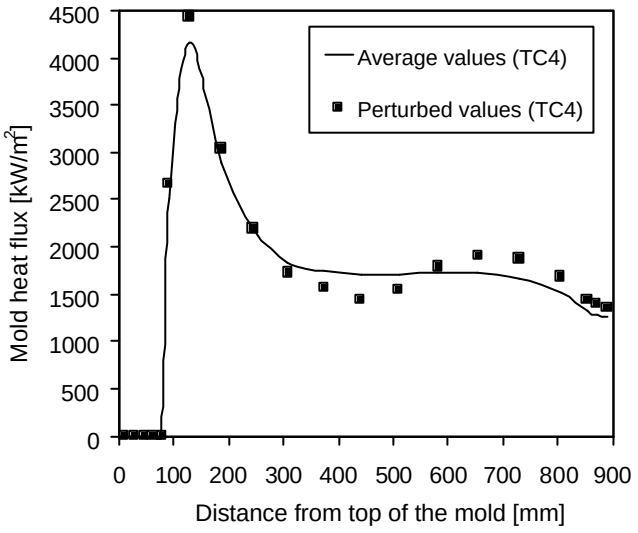

Figure 2: CCAST. Results of the stability test for a thermocouple line (TC4)

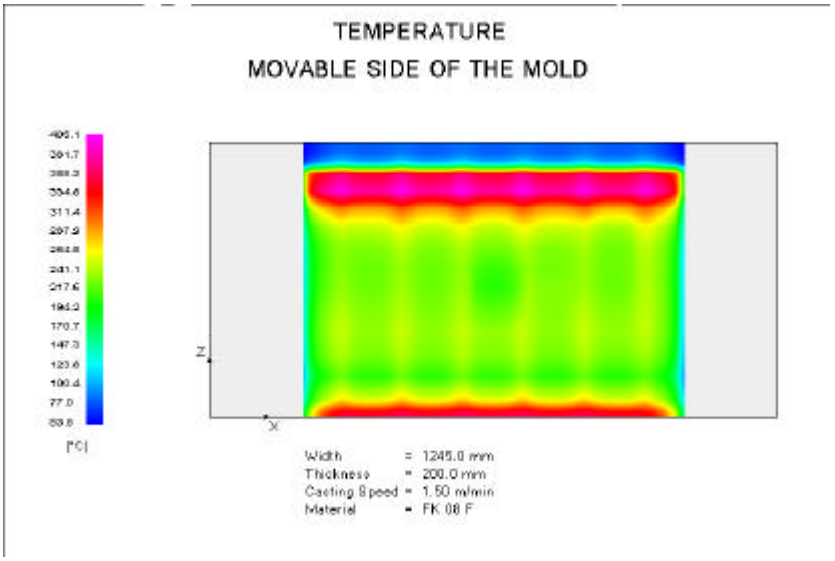

Figure 3: Hot face of the movable mold plate. Temperature map

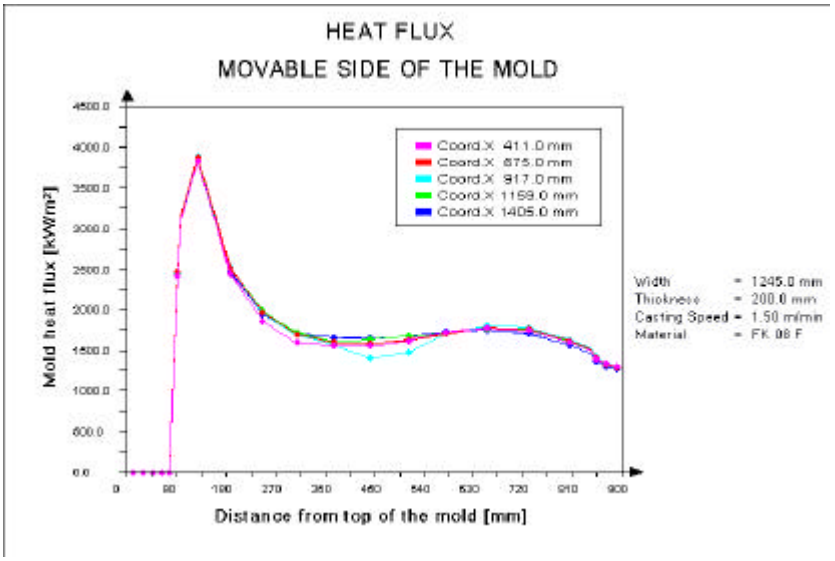

Figure 4: Heat fluxes along the movable mold plate

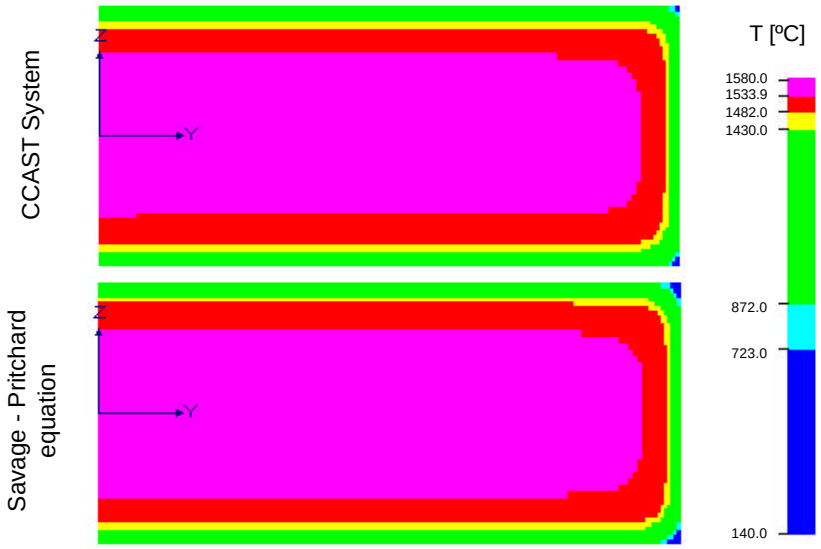

Figure 5: Comparison between the results obtained with the inverse analysis and with the Savage-Pritchard equation

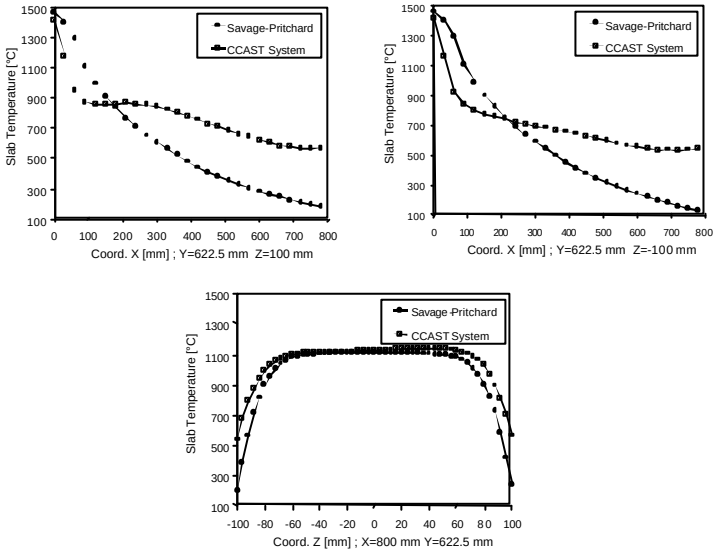

Figure 6: Comparison between the results obtained with the inverse analysis and with the Savage-Pritchard equation. Corner area detail

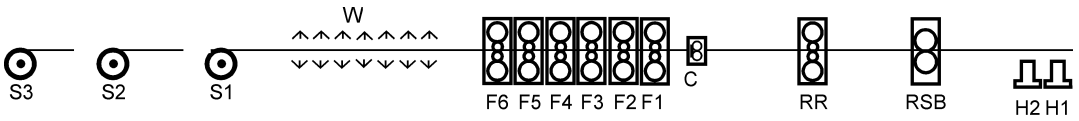

C : crop shear
F1, F2, F3, F4, F5, F6 : finishing stands
W : water cooling
S1, S2, S3 : sheet coilers

RSB : roughing scale breaker
RR : reversible roughing stand
H1, H2 : re-heating furnaces

Figure 7: Hot rolling mill

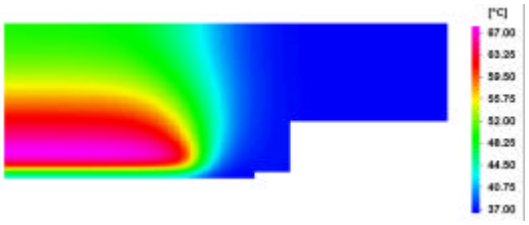

beginning of selected coil rolling

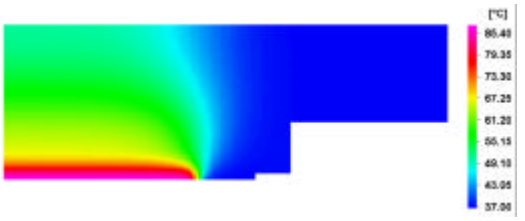

ending of selected coil rolling

a) temperature maps of the F1 working rolls

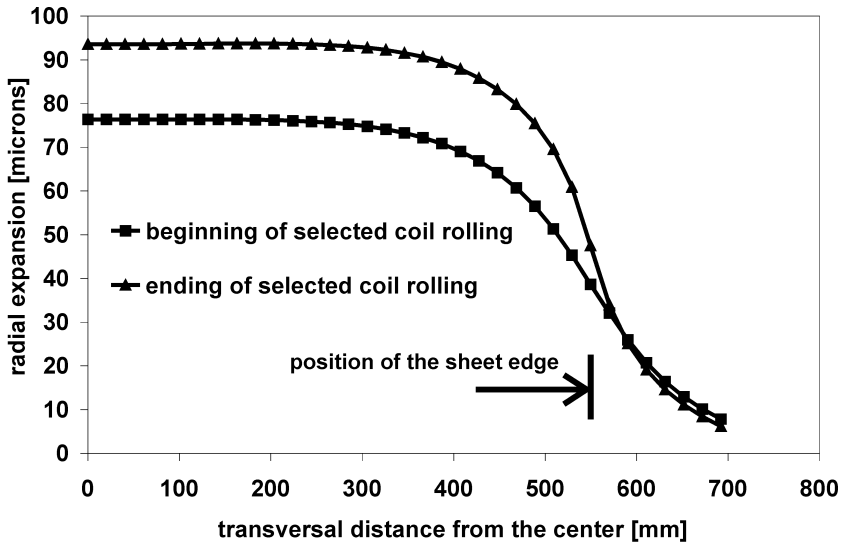

b) thermal expansion of work rolls

Figure 8: Analysis of the stand F1

Figure 9: Analysis of the F1 stand. Fixed mesh and pseudo-concentrations distribution

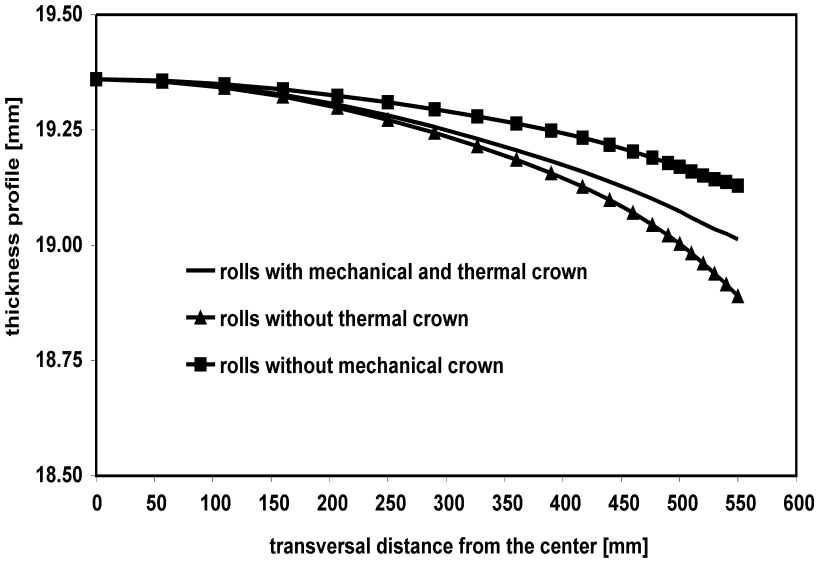

Figure 10: Parametric analysis of the F1 stand

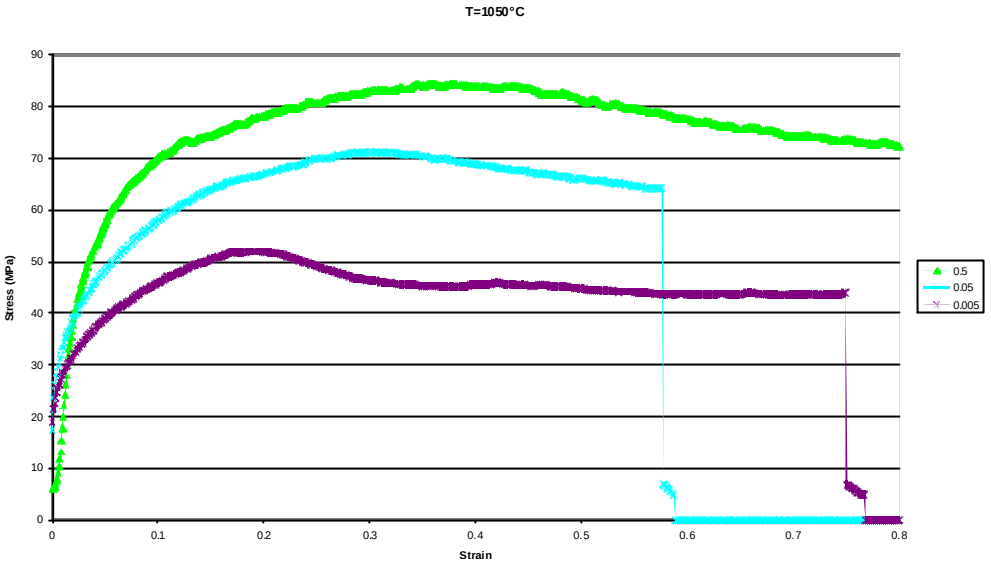

Figure 11: Compression tests performed at 0.005, 0.05 and 0.5 1/sec

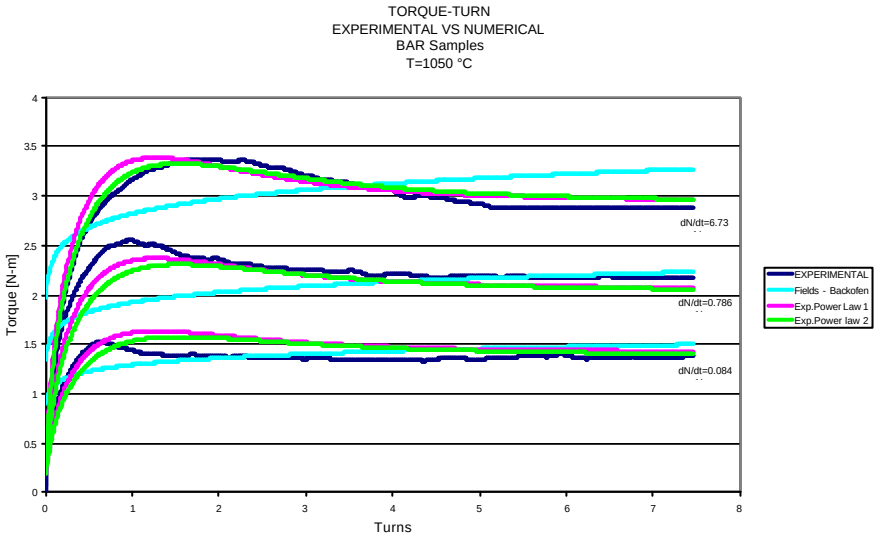

Figure 12: Torsion tests

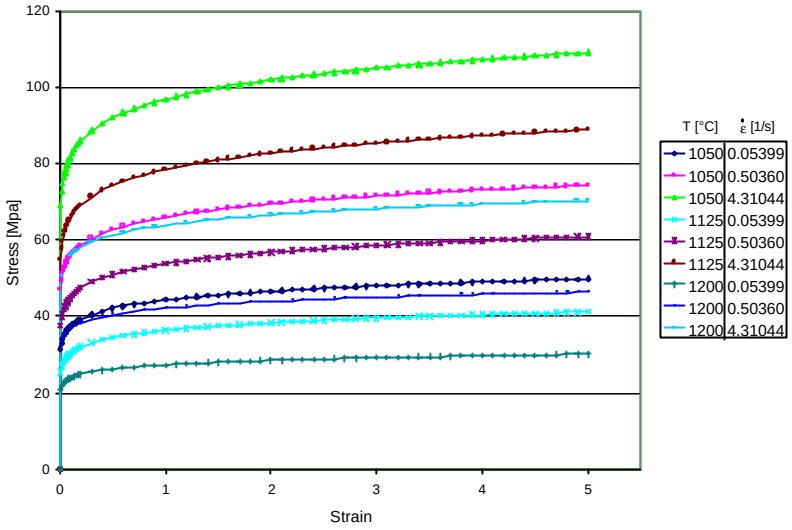

Figure 13: Post-processing of the torsion test results. Fields-Backofen model

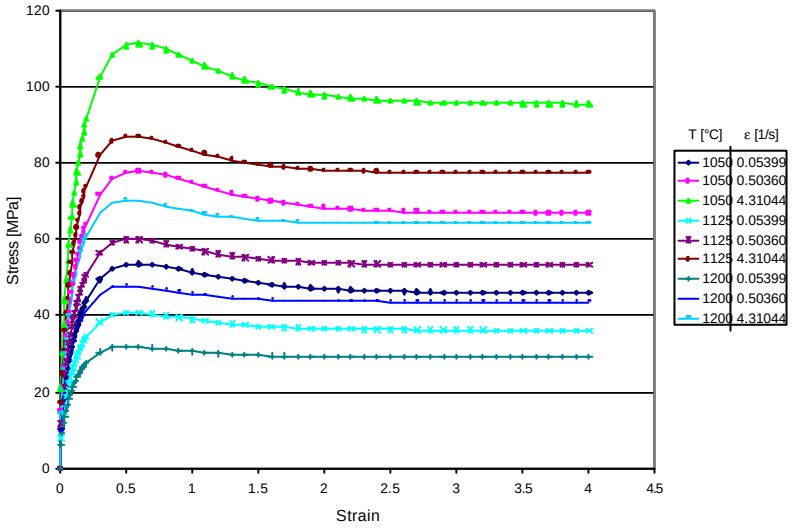

Figure 14: Post-processing of the torsion test results. Exponential-power law 1

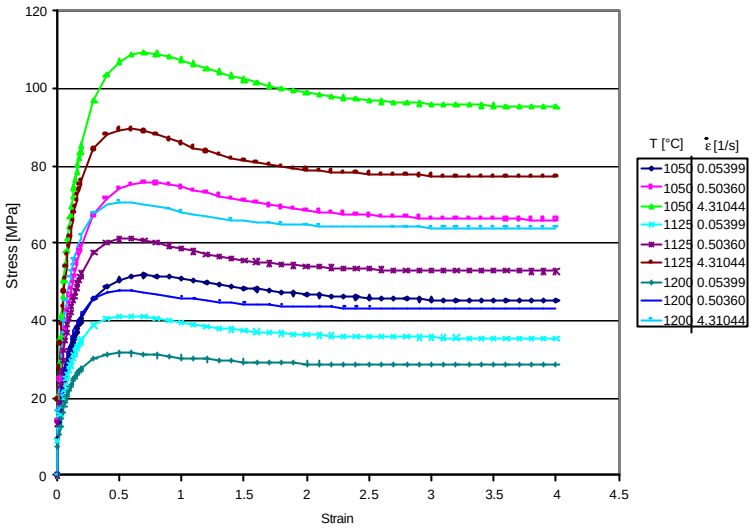

Figure 15: Post-processing of the torsion test results. Exponential-power law 2

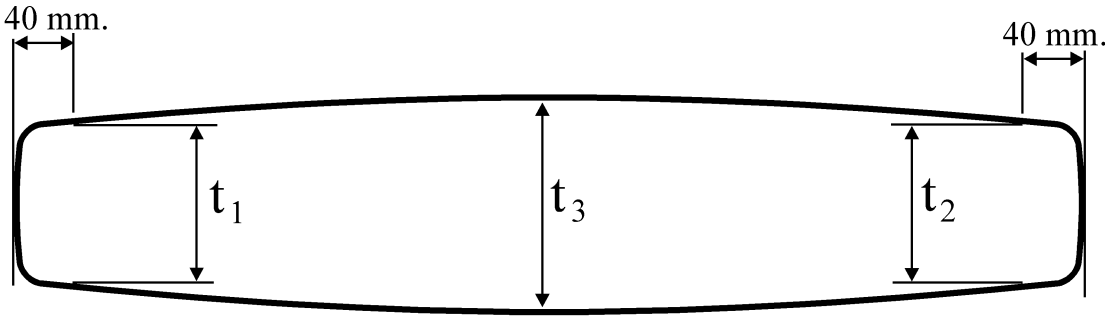

Not to scale

$$\text{plate crown} = t_3 - 0.5\,(t_1 + t_2)$$

Figure 16: Definition of plate crown

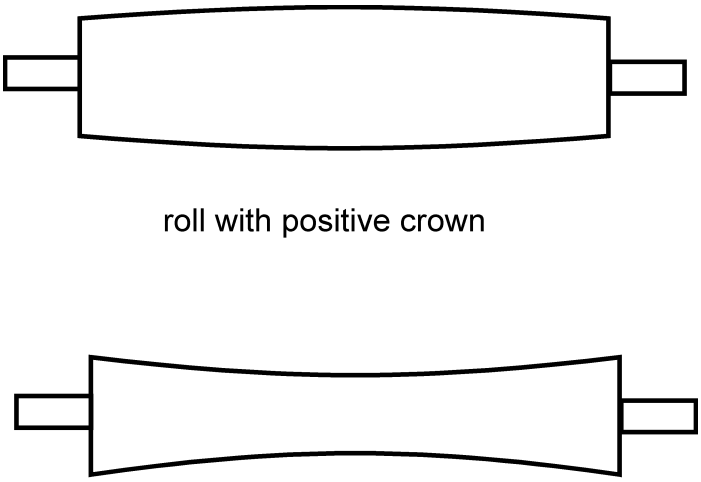

Figure 17: Roll crowns